The effects of Er^{3+} ion concentration on 2.0-μm emission performance in Ho^{3+}/Tm^{3+} co-doped $Na_5Y_9F_{32}$ single crystal under 800-nm excitation

Benli Ding(丁本利), Xiong Zhou(周雄), Jianli Zhang(章践立), Haiping Xia(夏海平), Hongwei Song(宋宏伟), and Baojiu Chen(陈宝玖)

Citation: Chin. Phys. B, 2021, 30 (**1**): 017801. DOI: 10.1088/1674-1056/abaede
Journal homepage: http://cpb.iphy.ac.cn; http://iopscience.iop.org/cpb

What follows is a list of articles you may be interested in

Cascaded plasmonic nanorod antenna for large broadband local electric field enhancement

Dou Zhang(张豆), Zhong-Jian Yang(杨中见), Jun He(何军)
Chin. Phys. B, 2019, 28 (**10**): 107802. DOI: 10.1088/1674-1056/ab3f99

Substitution priority of Eu^{2+} in multi-cation compound $Sr_{0.8}Ca_{0.2}Al_2Si_2O_8$ and energy transfer

Zhi-Ping Yang(杨志平), Zhen-Ling Li(李振玲), Zhi-Jun Wang(王志军), Pan-Lai Li(李盼来), Miao-Miao Tian(田苗苗), Jin-Ge Cheng(程金阁), Chao Wang(王超)
Chin. Phys. B, 2018, 27 (**1**): 017802. DOI: 10.1088/1674-1056/27/1/017802

2.0-μm emission and energy transfer of Ho^{3+}/Yb^{3+} co-doped $LiYF_4$ single crystal excited by 980 nm

Yang Shuo, Xia Hai-Ping, Jiang Yong-Zhang, Zhang Jia-Zhong, Jiang Dong-Sheng, Wang Cheng, Feng Zhi-Gang, Zhang Jian, Gu Xue-Mei, Zhang Jian-Li, Jiang Hao-Chuan, Chen Bao-Jiu
Chin. Phys. B, 2015, 24 (**6**): 067802. DOI: 10.1088/1674-1056/24/6/067802

Concentration effect of the near-infrared quantum cutting of 1788-nm luminescence of Tm^{3+} ion in $(Y_{1-x}Tm_x)_3Al_5O_{12}$ powder phosphor

Chen Xiao-Bo, Li Song, Ding Xian-Lin, Yang Xiao-Dong, Liu Quan-Lin, Gao Yan, Sun Ping, Yang Guo-Jian
Chin. Phys. B, 2014, 23 (**8**): 087809. DOI: 10.1088/1674-1056/23/8/087809

Up-conversion luminescence properties and energy transfer of Er^{3+}/Yb^{3+} co-doped oxyfluoride glass ceramic containing CaF_2 nano-crystals

Ma Chen-Shuo, Jiao Qing, Li Long-Ji, Zhou Da-Cheng, Yang Zheng-Wen, Song Zhi-Guo, Qiu Jian-Bei
Chin. Phys. B, 2014, 23 (**5**): 057802. DOI: 10.1088/1674-1056/23/5/057802

The effects of Er^{3+} ion concentration on 2.0-μm emission performance in Ho^{3+}/Tm^{3+} co-doped $Na_5Y_9F_{32}$ single crystal under 800-nm excitation*

Benli Ding(丁本利)[1], Xiong Zhou(周雄)[1], Jianli Zhang(章践立)[1], Haiping Xia(夏海平)[1,†], Hongwei Song(宋宏伟)[2], and Baojiu Chen(陈宝玖)[3]

[1] *Key Laboratory of Photo-electronic Materials, Ningbo University, Ningbo* 315211, *China*
[2] *State Key Laboratory on Integrated Optoelectronics, College of Electronic Science and Engineering and College of Physics, Jilin University, Changchun* 130012, *China*
[3] *Department of Physics, Dalian Maritime University, Dalian* 116026, *China*

(Received 25 June 2020; revised manuscript received 8 August 2020; accepted manuscript online 13 August 2020)

$Na_5Y_9F_{32}$ single crystals doped with ∼ 0.8-mol% Ho^{3+}, ∼ 1-mol% Tm^{3+}, and various Er^{3+} ion concentrations were prepared by a modified Bridgman method. The effects of Er^{3+} ion concentration on 2.0-μm emission excited by an 800-nm laser diode were investigated with the help of their spectroscopic properties. The intensity of 2.0-μm emission reached to maximum when the Er^{3+} ion concentration was ∼ 1 mol%. The energy transfer mechanisms between Er^{3+}, Ho^{3+}, and Tm^{3+} ions were identified from the change of the absorption spectra, the emission spectra, and the measured decay curves. The maximum 2.0-μm emission cross section of the $Er^{3+}/Ho^{3+}/Tm^{3+}$ tri-doped $Na_5Y_9F_{32}$ single crystal reached 5.26×10^{-21} cm^2. The gain cross section spectra were calculated according to the absorption and emission cross section spectra. The cross section for ∼ 2.0-μm emission became a positive gain once the inversion level of population was reached 30%. The energy transfer efficiency was further increased by 11.81% through the incorporation of Er^{3+} ion into Ho^{3+}/Tm^{3+} system estimated from the measured lifetimes of Ho^{3+}/Tm^{3+}- and $Er^{3+}/Ho^{3+}/Tm^{3+}$-doped $Na_5Y_9F_{32}$ single crystals. The present results illustrated that the $Er^{3+}/Ho^{3+}/Tm^{3+}$ tri-doped $Na_5Y_9F_{32}$ single crystals can be used as promising candidate for 2.0-μm laser.

Keywords: 2.0-μm emission, $Er^{3+}/Ho^{3+}/Tm^{3+}$, energy transfer, $Na_5Y_9F_{32}$ single crystal

PACS: 78.60.Lc, 78.55.Hx **DOI:** 10.1088/1674-1056/abaede

1. Introduction

In recent decades, ∼ 2.0-μm infrared laser single crystals based on Tm^{3+} and Ho^{3+} as the central luminous ions have been received extensive attention owing to their both prominent physical–chemical properties and high emission efficiency beneficial from periodic lattice field structure of three-dimensional symmetry.[1–4] Previously studied single crystals were mainly concentrated on oxide ones.[5] The oxide single crystals have drawbacks of the low transmittance in the range of infrared and low luminous efficiency due to high matrix phonon energy.[6] In contrast, the fluorides have attracted substantial attention because of its lower phonon energy and higher transparency. The $Na_5Y_9F_{32}$ is a newly developed fluoride single crystal.[7] It possesses excellent thermal stability, higher optical transparency in the range of infrared and optical performance, and is easy for trivalent rare-earth ions to replace the Y^{3+} ions. These excellent properties make it very suitable as potential laser matrix for 2.0-μm infrared laser devices. Compared with the cubic $NaYF_4$ crystal, $Na_5Y_9F_{32}$ crystal may possess better thermal stability. Although both $Na_5Y_9F_{32}$ and cubic $NaYF_4$ crystals belong to fluorite cubic system, in which Na^{3+} and Y^{3+} ions are randomly distributed in the cationic positions in the center of the cube, there are still obvious differences in crystal structure resulting into their different properties. For the $Na_5Y_9F_{32}$ crystal, the dodecahedrons and octahedrons are formed by coordinated by 8 and 6 numbers of F^- ions. Both Na^+ and Y^{3+} are located in the dodecahedral sites, while the octahedrons are in vacant. The octahedral vacancies may provide a possible buffer space for the ion vibration resulting into the thermal stability.[8] While for cubic $NaYF_4$, the cation sites are mainly occupied by Na^+ and Y^{3+}, adjacent to F^-, and each Na^+ or Y^{3+} is coordinated by 8 number of F^- ions to form a dodecahedron.[9]

As we all know, the energy level transition of Ho^{3+} : $^5I_7 \rightarrow {}^5I_8$ or Tm^{3+} : $^3F_4 \rightarrow {}^3H_6$ can obtain ∼ 2.0-μm emission. For Ho^{3+} ion-doped single crystal, the operation of tunable laser can extend to ∼2.1 μm, while for Tm^{3+}-doped single crystal, the tunable range can only be extended from 1.85 μm to 2.03 μm. Moreover, Ho^{3+} ion generally has a higher emission cross section and a longer lifetime of higher laser energy levels compared to Tm^{3+} ion, and these features are conducive

*Project supported by the National Natural Science Foundation of China (Grant No. 51772159), the Natural Science Foundation of Zhejiang Province, China (Grant No. LZ17E020001), the Natural Science Foundation of Ningbo City (Grant No. 202003N4099), and K C Wong Magna Fund in Ningbo University.

†Corresponding author. E-mail: hpxcm@nbu.edu.cn

to low-threshold and efficient laser operation.[10,11] However, there is still a tough task due to the lack of suitable absorption bands for Ho^{3+} ion that cannot directly absorb the most common commercial laser diodes at the pumping beam of 800 nm or 980 nm.[12] Therefore, some corresponding sensitizers such as Er^{3+}, Tm^{3+}, and Yb^{3+} ions are taken into consideration to absorb pumping energy effectively due to they have strong absorption band near 800-nm wavelength (Er^{3+} or Tm^{3+} ion) and near 980-nm wavelength (Er^{3+} or Yb^{3+} ion).[13] Previous researches have demonstrated that single crystal co-doped or tri-doped with sensitizer ions and Ho^{3+} can lead to an increase in emission intensity of 2.0 μm, and the energy transfer mechanisms between Ho^{3+} ion and sensitizer ions have also been studied in Ho^{3+}/Er^{3+}, Ho^{3+}/Yb^{3+}, Ho^{3+}/Tm^{3+} co-doped, and $Ho^{3+}/Er^{3+}/Yb^{3+}$ tri-doped single crystals.[14–17] Nevertheless, there is no investigation about the 2.0-μm emission of fluoride single crystal tri-doped with $Er^{3+}/Tm^{3+}/Ho^{3+}$.

In this work, we report the further enhanced 2.0-μm emission by addition of Er^{3+} in the Tm^{3+}/Ho^{3+} co-doped $Na_5Y_9F_{32}$ single crystals. The 2.0-μm emission characteristics and energy transfer mechanism were analyzed. The absorption cross sections and emission cross sections were determined to evaluate the spectral performance.

2. Experimental

An improved Bridgman method was used to grow the $Na_5Y_9F_{32}$ single crystals under the condition of using KF as a flux. The commercial KF, YF_3, NaF, HoF_3, ErF_3, and TmF_3 powders with 99.99% high purity were prepared as raw materials to grow $Na_5Y_9F_{32}$ single crystals according to the following molar composition: 30 NaF-18 KF-$(50.2-\chi)$ YF_3-χ ($\chi = 1, 2, 3$) ErF_3-0.8 HoF_3-1 TmF_3. The 0.8-mol% Ho^{3+} singly doped, 0.8-mol% Ho^{3+}/1-mol% Tm^{3+} co-doped, 0.8-mol% Ho^{3+}/0.5 mol% Er^{3+} co-doped, χ-mol% ($\chi = 1, 2, 3$) Er^{3+}/0.8-mol% Ho^{3+}/1-mol% Tm^{3+} tri-doped $Na_5Y_9F_{32}$ single crystals were denoted as NYF-H, NYF-HT, NYF-HE, and NYF-HTEχ, respectively. The specific growth processes of $Na_5Y_9F_{32}$ single crystal were described in Ref. [7].

The obtained single crystals were cut and then polished to the thickness of 2 mm for the spectral and optical measurements as shown in Fig. 2(e). The real Tm^{3+}, Ho^{3+}, and Er^{3+} ions concentrations in $Na_5Y_9F_{32}$ single crystals were recorded by ICP (Inductive Coupled Plasma Emission Spectrometer). Table 1 illustrated the doping concentrations of Tm^{3+}, Ho^{3+}, and Er^{3+} ions in the raw materials and the measured concentrations of Tm^{3+}, Ho^{3+}, and Er^{3+} ions in the synthesized crystal. A Bruker D8 Advance (Germany) was used to record the x-ray diffraction (XRD). A Cary 5000 UV/VIS/NIR spectrophotometer (Agilent Co., America) was used to measure the absorption spectra. The emission spectra and decay curves of the prepared single crystals were obtained by an FLSP 920-type spectrometer (Edinburgh Co., England). All of the above measurements were performed at room temperature.

3. Results and discussion

3.1. EDS and XRD analyses

Figures 1(a) and 1(b) show the scanning electron microscope (SEM) image and energy dispersive x-ray spectroscopy (EDS) analysis of the NYF-HTE0.5 crystal. It can be seen from the SEM image of Fig. 1(a) that the polished single crystal shows a smooth surface at a magnification of 10000. The EDS analysis of Fig. 1(b) shows that the composition of the single crystal is very close to the nominal $Na_5Y_9F_{32}$ composition and the $Na_5Y_9F_{32}$ single crystal is mainly composed of F, Na, Y, Ho, Er, Tm and a small amounts of K. The detection of K ion signal in the EDS analysis is believed due to a small amount of K residue as a flux in crystal growth. Figures 1(c)–1(h) display the color mappings of all the elements in the NYF-HTE0.5 crystal.

Figures 2(b)–2(d) show the XRD patterns of NYF-H, NYF-HE, and NYF-HTE0.5 crystals. According to the PDF cards (27-1428), as shown in Fig. 2(a), the diffraction peak position of the obtained single crystal sample doped with Er^{3+}, Ho^{3+}, Tm^{3+} ions completely matches the diffraction peak position of the standard $Na_5Y_9F_{32}$. In addition, the cell parameters can be calculated by[18]

$$d = \frac{a}{\sqrt{h^2 + k^2 + l^2}}. \tag{1}$$

The calculated cell parameters of the NYF-HTE0.5 single crystals are $a = b = c = 0.5545$ nm from the measured XRD pattern.

Table 1. Molar fractions of Er^{3+}, Ho^{3+}, and Tm^{3+} in raw material and measured concentrations of Er^{3+}, Ho^{3+}, and Tm^{3+} ions in $Na_5Y_9F_{32}$ single crystals.

Sample	NYF-H	NYF-HT	NYF-HE	NYF-HTE0.5	NYF-HTE1	NYF-HTE2
Er^{3+} (mol% in raw material)	0	0	0.5	0.5	1	2
Measured Er^{3+} (mol% in crystal)	–	–	0.513	0.513	1.024	2.046
Ho^{3+} (mol% in raw material)	0.8	0.8	0.8	0.8	0.8	0.8
Measured Ho^{3+} (mol% in crystal)	0.797	0.797	0.798	0.798	0.797	0.798
Tm^{3+} (mol% in raw material)	0	1	0	1	1	1
Measured Tm^{3+} (mol% in crystal)	–	1.014	–	1.014	1.014	1.014

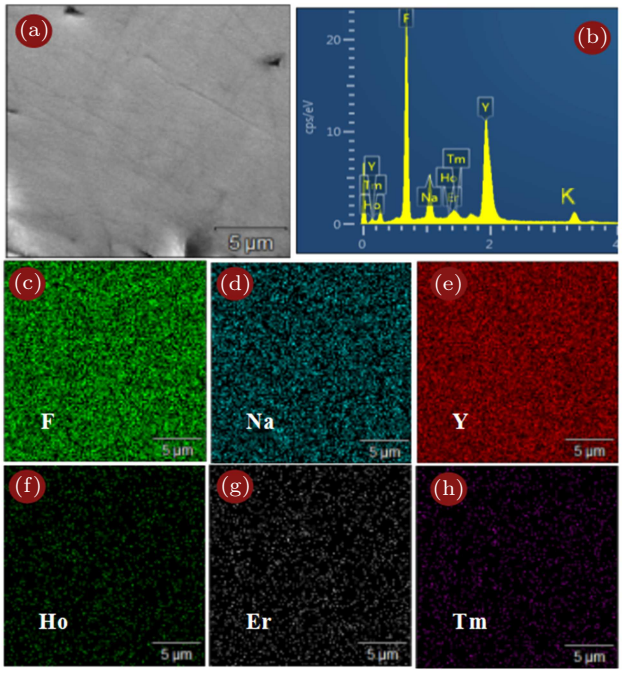

Fig. 1. (a) The SEM image of the NYF-HTE0.5 crystal; (b) the EDS analysis of the the NYF-HTE0.5 crystal, and (c)–(h) elemental mappings for the NYF-HTE0.5 crystal.

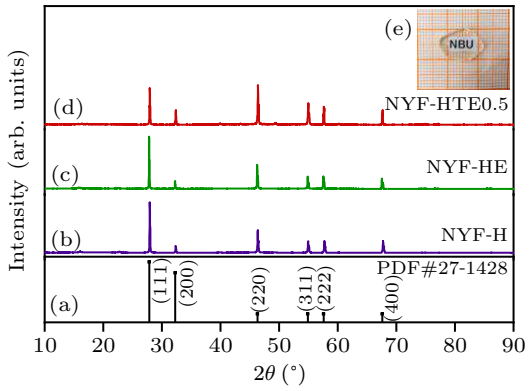

Fig. 2. XRD patterns of (a) the standard data for $Na_5Y_9F_{32}$ crystal; (b) NYF-H crystal; (c) NYF-HE crystal; (d) NYF-HTE0.5 crystal; (e) the photos of NYF-HTE0.5 crystal polished slices.

3.2. Absorption spectra and absorption cross section spectra

Figure 3 illustrates the absorption spectra of the NYF-H, NYF-HE, and NYF-HTE0.5 crystals in the wavelength of 400 nm–2200 nm. In order to eliminate the influence of sample thickness, the absorbance is converted into absorption coefficient α according to the following formula:

$$\alpha = 2.303A/L, \tag{2}$$

where A and L are the absorbance and the thickness of the single crystal, respectively. The absorption bands of Ho^{3+}, Er^{3+}, and Tm^{3+} are also labeled in Fig. 3, which is consistent with transitions from the ground state to higher energy levels. For Ho^{3+} singly doped NYF-H crystal, the absorption peaks corresponding to the Ho^{3+} ion transitions from the $^5I_8$ ground state to the higher levels $^5G_5$, $^5F_1/^5G_6$, $^5F_3$, $^5S_2/^5F_4$,$^5F_5$, $^5I_6$, $^5I_7$ located in the characteristic wavelength of 413, 446, 480, 535, 642, 1153, 1929 nm, are observed. While for the Ho^{3+}, Er^{3+} co-doped NYF-HE one, it can be observed the Er^{3+} characteristic absorption consisting of seven main bands centered at 485, 516, 538, 639, 800, 973, 1515 nm, which is attributed to the Er^{3+} transitions from $^4F_{13/2}$ to $^4F_{2/7}$, $^4H_{11/2}$,$^4S_{3/2}$, $^4F_{9/2}$,$^4I_{9/2}$, $^4I_{11/2}$, $^4I_{13/2}$, respectively besides the absorption bands of Ho^{3+} ion. In addition to the absorption peaks of Er^{3+} and Ho^{3+}, there appear new four absorption bands at 681, 798, 1197, and 1637 nm which is attributed to the transitions from $^3H_6$ to $^3S_{2,3}$, $^3H_4$, $^3H_5$, and $^3F_4$ of Tm^{3+} ion in the Ho^{3+}, Tm^{3+}, and Er^{3+} triply doped NYF-HTE0.5 crystal. It can be confirmed from Figs. 1 and 2 that the Ho^{3+}, Tm^{3+}, and Er^{3+} rare-earths ions are effectively introduced into the crystal lattices of $Na_5Y_9F_{32}$ crystals. In addition, there appear strong absorption bands at 800 nm (Er^{3+} : $^4F_{15/2} \rightarrow {}^4I_{9/2}$ and Tm^{3+} : $^3H_6 \rightarrow {}^3H_4$) and 980 nm ($Er^{3+}$: $^4F_{15/2} \rightarrow {}^4I_{11/2}$) which are very favorable for using commercial LEDs at 800-nm and 980-nm wavelengths as pumping sources.[19]

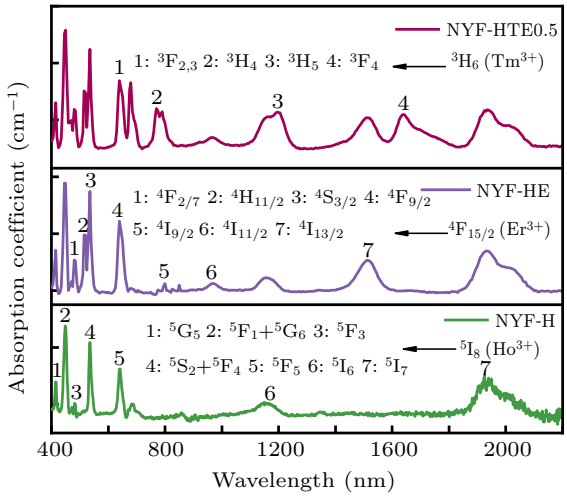

Fig. 3. Optical absorption spectra of NYF-H, NYF-HE, NYF-HTE0.5 crystals.

The absorption and emission cross sections at 2.0 μm are usually measured to clarify the energy transfer mechanism between the Er^{3+}, Tm^{3+}, and Ho^{3+} ions. According to the absorption spectra of $Na_5Y_9F_{32}$ single crystal illustrated in Fig. 3, the absorption cross section at 2.0 μm can be calculated by[20]

$$\sigma_{abs}(\lambda) = \frac{2.303\log(I_0/I)}{NL} = \frac{\alpha}{N}, \tag{3}$$

where I_0 and I are intensity of the incident optical and optical intensity throughout the crystals, respectively. L, N, and α are the thickness of the crystal, the concentration of rare earth ion, and the absorption coefficient, respectively. Figure 4 illustrates the calculated absorption cross sections of the Ho^{3+} : $^5I_7 \rightarrow {}^5I_8$ transition. As shown in the figure, the maximum absorption cross sections of NYF-HTE1 crystal reaches 2.86×10^{-21} cm^2.

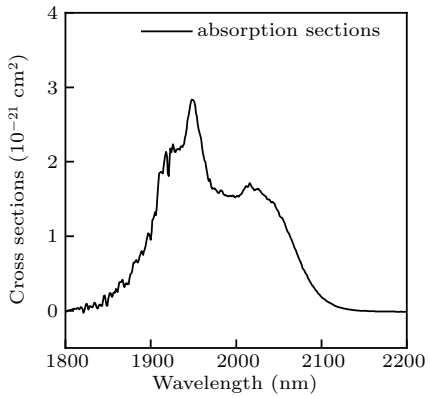

Fig. 4. Absorption cross-section spectra of the Ho^{3+} : $^5I_7 \rightarrow {}^5I_8$ transition in NYF-HTE1 crystal.

3.3. Emission spectra and emission cross section spectra

Figure 5(a) illustrates the fluorescence spectra of χEr/0.8Ho/1Tm ($\chi = 0$, 0.5, 1, and 2) doped $Na_5Y_9F_{32}$ crystals in the range of 1400 nm–2200 nm under excitation at 800 nm, and figures 5(b) and 5(c) show the intensity at 2.0 μm, 1.47 μm, 1.53 μm, and 1.64 μm as change of the Er^{3+} concentrations. Figures 6(a) and 6(b) display the fluorescence spectra of χEr/0.8Ho/1Tm ($\chi = 0$, 0.5, 1, and 2) tri-doped $Na_5Y_9F_{32}$ crystals in the 2500 nm–2900 nm band and the intensity at 2.7 μm and 2.8 μm as change of Er^{3+} concentration. In addition, the relative fluorescence intensity of the ordinate in Figs. 5(a) and 6(a) is the fluorescence intensity obtained by measurement. As shown in Fig. 5(a), there are main four emission peaks centered at 2 μm, 1.64 μm, 1.53 μm, 1.47 μm, while in Fig. 6(b), two peaks at 2.7 μm and 2.8 μm. The intensity of emission bands at 1.64 μm, 1.53 μm is extremely weak in all four samples as shown in insert of Fig. 5(a). The emissions at 2.0 μm and 2.8 μm come from the transitions of Ho^{3+} : $^5I_7 \rightarrow {}^5I_8$ and Ho^{3+} : $^5I_6 \rightarrow {}^5I_7$, respectively. The emissions at 1.53 μm and 2.7 μm correspond to the transitions of Er^{3+} : $^4I_{13/2} \rightarrow {}^4I_{15/2}$ and Er^{3+} : $^4I_{11/2} \rightarrow {}^4I_{13/2}$, respectively. The other emissions at 1.47 μm and 1.64 μm arise from Tm^{3+} : $^3H_4 \rightarrow {}^3F_4$ and Tm^{3+}: $^3F_4 \rightarrow {}^3H_6$ transitions, respectively. As shown in Figs. 5(b), 5(c), and 6(b), by contrast of NYF-HT and NYF-HTEχ ($\chi = 0.5$, 1, and 2) crystals, it is apparent that the 1.53-μm, 1.64-μm, 2.0-μm, 2.7-μm, and 2.8-μm emission intensities of $Na_5Y_9F_{32}$ crystals increase gradually as increase of Er^{3+} concentration from 0 mol% to 1 mol%, and it reaches maximum when the Er^{3+} concentration is about $\sim$ 1 mol%, it decreases abruptly with Er^{3+} concentration ranging from 1 mol% to 2 mol%. However, the fluorescence intensity of 1.47 μm gradually decreases as increase of the Er^{3+} ion concentration. In addition, the peak intensity ratio values of 2.0 μm to 1.64 μm and 2.0 μm 1.53 μm in NYF-HT and NYF-HTEχ crystals are also shown in Table 2. The 2.0-μm fluorescence of NYF-HTE1 crystals possesses the maximum intensity in the present study, and the peak intensity ratios of 2.0 μm to 1.64 μm and 2.0 μm to 1.53 μm return to 50.22 and 59.09. It strongly indicates that the energy in Tm^{3+} : $^3F_4$ (1.64 μm) and Er^{3+} : $^4I_{13/2}$ (1.53 μm) levels mostly transfers sufficiently to the Ho^{3+} : $^5I_7$ level by emitting 2.0-μm emission. Besides, the values of the $I_{2.0}/I_{1.53}$, $I_{2.0}/I_{1.64}$ become larger as the concentration of Er^{3+} ion increases until the Er^{3+} concentration reaches 1 mol%. Therefore, the Er^{3+} ion is considered as an efficient sensitizer for improving 2.0-μm emission in Ho^{3+}, Tm^{3+} co-doped $Na_5Y_9F_{32}$ crystals, and the optimum doping combination concentrations of Er^{3+}, Ho^{3+}, and Tm^{3+} are about 1 mol%, 0.8 mol%, and 1 mol%.

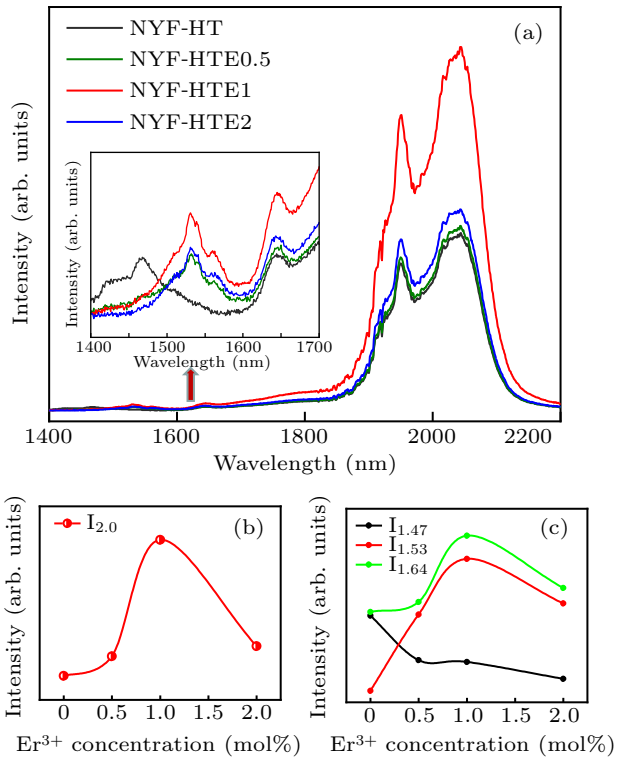

Fig. 5. (a) Emission spectra of NYF-HT, NYF-HTEχ ($\chi = 0.5$, 1, 2) crystals pumped at 800-nm LD, (b) the relationships between the 2.0-μm intensity and the concentration of Er^{3+}, (c) the relationships between the 1.47-μm, 1.53-μm, and 1.53-μm intensities and the concentration of Er^{3+}.

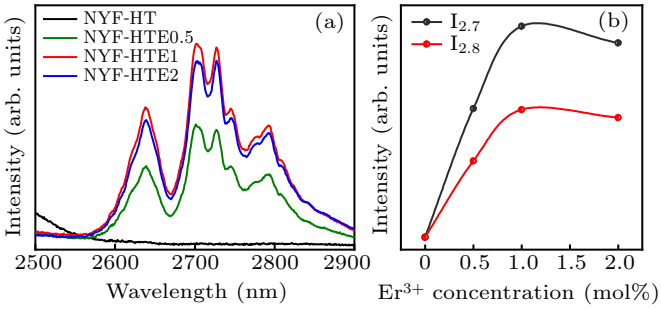

Fig. 6. Emission spectra of NYF-HT, NYF-HTEχ ($\chi = 0.5$, 1, 2) crystals pumped at 800-nm LD, (b) the relationships between the 2.7-μm, 2.8-μm intensities and the concentration of Er^{3+}.

Table 2. The intensity ratios of $I_{2.0/I1.53}$, $I_{2.0/I1.64}$ in NYF-HT, NYF-HTEχ ($\chi = 0.5$, 1, 2) crystals.

Sample	NYF-HT	NYF-HTE0.5	NYF-HTE1	NYF-HTE2
$I_{2.0/1.53}$	–	48.59	59.09	48.30
$I_{2.0/1.64}$	46.78	46.80	50.22	42.57

The emission cross section can be obtained from the calculated absorption cross section by using the McCumber formula as follows:[21]

$$\sigma_{\rm em}(\lambda) = \sigma_{\rm abs}(\lambda)\frac{Z_{\rm l}}{Z_{\rm u}}\exp\left(\frac{E_{\rm zl} - hc/\lambda}{KT}\right), \tag{4}$$

where $Z_{\rm l}$ and $Z_{\rm u}$ represent the partition functions of the lower level (Ho^{3+} : $^5I_8$) and the upper level (Ho^{3+}: $^5I_7$), respectively; T, K are room temperature and the Boltzmann constant, respectively; h, λ, c, and $E_{\rm zl}$ denote Planck constant, transition (Ho^{3+} : $^5I_7 \rightarrow {}^5I_8$) wavelength, light velocity, and zero-line energy, respectively.

Figure 7 illustrates the calculated emission cross sections of the Ho^{3+} : $^5I_7 \rightarrow {}^5I_8$ transition. As shown in the figure, the maximum emission cross sections of NYF-HTE1 crystal reaches 5.26×10^{-21} cm^2. The obtained emission cross section of $Na_5Y_9F_{32}$ single crystal is larger than those in tellurite glass (4.52×10^{-21} cm^2),[22] fluoride glass (2.47×10^{-21} cm^2)[23] and germanate glass (4×10^{-21} cm^2).[24] The laser effect would benefit from the $Na_5Y_9F_{32}$ single crystal of high emission cross-section as host material, indicating that the Er^{3+}/Ho^{3+}/Tm^{3+} tri-doped $Na_5Y_9F_{32}$ single crystal is a potentially useful material for 2.0-μm applications.

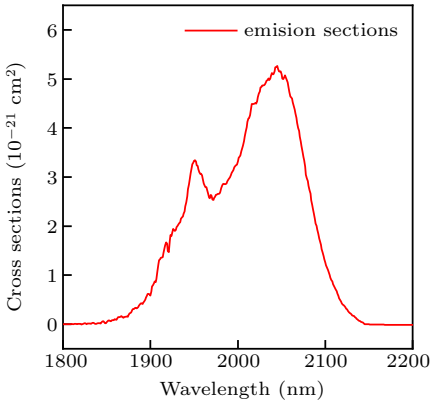

Fig. 7. Emission cross-section spectra of the Ho^{3+} : $^5I_7 \rightarrow {}^5I_8$ transition in NYF-HTE1 crystal.

3.4. Gain cross section spectra

On the basis of the obtained absorption cross section and emission cross section, the optical gain coefficient $g(\lambda)$ as a function of population inversion for the upper laser state can be calculated and defined as[25]

$$g(\lambda) = N_2\sigma_{\rm em} - N_1\sigma_{\rm abs}, \tag{5}$$

where N_2 and N_1 are the population inversion volume-densities of the upper level (Ho^{3+} : $^5I_7$) and lower level (Ho^{3+} : $^5I_7$), respectively. The inversion volume-density of total population is $N = N_2 + N_1$, and therefore the gain cross section spectrum $G(\lambda)$ can be estimated by

$$G(\lambda) = P\sigma_{\rm em} - (1-P)\sigma_{\rm abs}, \tag{6}$$

where P is the proportion of population inversion, and $0 \leq P \leq 1$. Figure 8 shows the gain cross sections of Ho^{3+} : $^5I_7 \rightarrow {}^5I_8$ transition in NYF-HTE1 crystal based on a function of different$P$ values and wavelengths. The value of P increases gradually from 0 to 1, with an increment of 0.1. As shown in Fig. 8, a positive gain is obtained when $P > 0.3$. It is confirmed that the gain band extends to longer wavelength and the gain coefficient increases with the increased value of P. In addition, it can be noticed that the pumping threshold of 2.0-μm laser is lower, which is advantageous for the 2.0-μm laser.

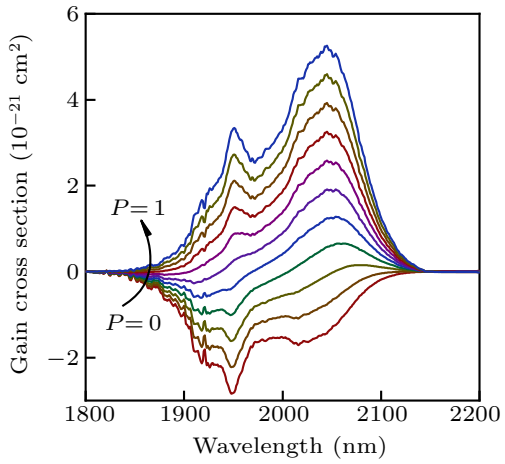

Fig. 8. Gain cross-section spectra of the Ho^{3+} : $^5I_7 \rightarrow {}^5I_8$ transition in NYF-HTE1 crystal.

3.5. Energy transfer mechanics and fluorescence decay curves

The possible energy transfer mechanisms of Ho^{3+}/Tm^{3+} and Ho^{3+}/Er^{3+}/Tm^{3+} in matrixes under the excitation of 800-nm LD have already reported[26] and are illustrated in Figs. 9(a) and 9(b), respectively. As shown in Fig. 9(a), in Ho^{3+}/Tm^{3+} co-doped $Na_5Y_9F_{32}$ single crystal, the Tm^{3+} ions are excited from the ground $^3H_6$ level to the excited $^3H_4$ level, then part of the energy down to the $^3F_4$ state with emitting 1.47-μm fluorescence. However, most of the energy of $^3H_4$ level excite the Tm^{3+} ions at the $^3H_6$ level and obtain two Tm^{3+} ions at the $^3F_4$ level. This process can improve the pump quantum efficiency, which is called cross relaxation.[25] Then ions in the Tm^{3+} : $^3F_4$ level can relax to the lower $^3H_6$ level with 1.64-μm emission ($^3F_4 \rightarrow {}^3H_6$ + 1.64 μm) which can be observed in Fig. 5(a). It can be noted from the absorption spectra that the energy levels between Tm^{3+} : $^3F_4$ and Ho^{3+} : $^5I_7$ is 944 cm^{-1}. It suggests that the ET process occurs requiring only 2–3 phonons for bridging in the $Na_5Y_9F_{32}$ single crystal (the maximum matrix phonon energy is about 409 cm^{-1} [27]) and the energy transfer (ET) process from Tm^{3+} : $^3F_4$ to Ho^{3+}: $^5I_7$ easily tends to take place. It can be deduced that the majority of the ions in Tm^{3+} : $^3F_4$ level transfer energy to Ho^{3+} : $^5I_7$ resulting from the strong emission of 2.0 μm derived from the $^5I_7 \rightarrow {}^5I_8$ transition of Ho^{3+}.

When Er^{3+} ion was doped into Ho^{3+}/Tm^{3+} co-doped $Na_5Y_9F_{32}$ single crystal, besides the energy transfer process between Tm^{3+} and Ho^{3+} ions transitions discussed above, the energy transfer processes of Tm^{3+} and Er^{3+} as well as Er^{3+} and Ho^{3+} are exhibited and shown in Fig. 9(b). Excited by 800-nm LD, the Tm^{3+} ions are excited from the ground $^3H_6$ level to the excited $^3H_4$ level and energy transfer (ET6) to $^4I_{9/2}$ level of Er^{3+} ions. Meanwhile, the ground state of Er^{3+} ions are excited to $^4I_{9/2}$ by ground state absorption (GSA). The excited Er^{3+} ions in $^4I_{9/2}$ level transits to Ho^{3+} ions in $^5I_5$ level by the ET1 process, or decay to Er^{3+}: $^4I_{11/2}$, and then Er^{3+} : $^4I_{11/2}$ transition to Ho^{3+} : $^5I_6$ level through the ET5 process or decays radiatively to the next level of $^4I_{13/2}$ with 2.7-μm emission ($^4I_{9/2} \rightarrow {}^4I_{13/2}$ + 2.7 μm). The $^5I_5$ energy level of Ho^{3+} ions are attenuated to the $^5I_7$ energy level in two steps and produces an emission of 2.8 μm ($^5I_5 \rightarrow {}^5I_6$, $^5I_6 \rightarrow {}^5I_7$ + 2.8 μm). A part of the Er^{3+} ion of the $^4I_{13/2}$ level relaxes to the ground state $^4I_{15/2}$, generating an emission of 1.53 μm ($^4I_{13/2} \rightarrow {}^4I_{15/2}$ + 1.53 μm), while the other part of the Er^{3+} : $^4I_{13/2}$ level excites adjacent Tm^{3+} : $^3F_4$ and Ho^{3+} : $^5I_7$ levels by the ET2 and ET3 processes to attenuate to the ground state $^4I_{15/2}$ in a non-radiative manner. The relevant process is explained by the following process:

ET2: $^4I_{13/2}$ (Er^{3+})+$^5I_8$(Ho^{3+}) → $^4I_{15/2}$ (Er^{3+})+$^5I_7$(Ho^{3+}),

ET3: $^4I_{13/2}$ (Er^{3+})+$^3H_6$ (Tm^{3+}) → $^4I_{15/2}$ (Er^{3+})+$^3F_4$ (Tm^{3+}).

Finally, the emission at 2.0 μm is ascribed to the transition of Ho^{3+} : $^5I_7 \rightarrow {}^5I_8$.

It can be noted from Fig. 3 that the energy gaps between Er^{3+}: $^4I_{9/2}$ and Ho^{3+} : $^5I_5$ (ET1), Er^{3+}: $^4I_{13/2}$ and Ho^{3+} : $^5I_7$ (ET2), Er^{3+}: $^4I_{13/2}$ and Tm^{3+} : $^3F_4$(ET3), Tm^{3+}: $^3F_4$ and Ho^{3+} : $^5I_7$ (ET4), Er^{3+}: $^4I_{11/2}$ and Ho^{3+} : $^5I_6$ (ET5), Tm^{3+}: $^3H_4$ and Er^{3+} : $^4I_{9/2}$ (ET6) are 698 cm^{-1}, 1460 cm^{-1}, 516 cm^{-1}, 944 cm^{-1}, 1666 cm^{-1}, 0 cm^{-1}, respectively. The ET6 process does not require phonon assistance, so the probability of this process is 100%. Since the ET5 process needs to bridge ~4 phonons, this process may occur with only a small number of particles. The occurrence of ET1 and ET2 processes promotes the energy transfer between Tm^{3+} and Er^{3+}, Er^{3+} and Ho^{3+} ions, and enhances down conversion. The enhancement of down-conversion emission may lead to a weakened up-conversion process.

The processes of ET1, ET3, and ET4 are easier to occur than that of ET2, which is beneficial to obtain enhanced emissions of 1.64 μm, 2.0 μm, and 2.8 μm due to increasing the emission behaviors of the $^3F_4$ level of Tm^{3+}, $^5I_7$ level of Ho^{3+}, and $^5I_6$ level of Ho^{3+}. By adding Er^{3+} from 0 mol% to 2 mol%, the emission of 1.47 μm (Tm^{3+} : $^3H_4 \rightarrow {}^3F_4$) gradually decreases. This is mainly due to the weakening absorption of Tm^{3+} to 800-nm excitation light source. In addition, as addition of Er^{3+} from 0 mol% to 1 mol%, the emissions of 1.64 μm (Tm^{3+}: $^3F_4 \rightarrow {}^3H_6$), 2.0 μm ($Ho^{3+}$: $^5I_7 \rightarrow {}^5I_8$), and 2.8 μm ($Ho^{3+}$: $^5I_6 \rightarrow {}^5I_7$) increase gradually because of the increased ET1, ET2, and ET3 processes, while 1.53 μm (Er^{3+}: $^4I_{13/2} \rightarrow {}^4I_{15/2}$) and 2.7 μm ($Er^{3+}$: $^4I_{11/2} \rightarrow {}^4I_{13/2}$) increase mainly due to increasing the populations on Er^{3+} : $^4I_{9/2}$, Er^{3+}: $^4I_{11/2}$ and Er^{3+} : $^4I_{13/2}$. The Er^{3+} ion concentration further increase from 1 mol% to 2 mol% results in the reduction of the above emissions, which may be owing to the possible occurrence of rare earth ions concentration quenching and clustering when the Er^{3+} concentration reaches 1 mol%.[28] Consequently, optimizing Er^{3+} concentration doping is necessary to obtain 2.0-μm high emission in the $Er^{3+}/Ho^{3+}/Tm^{3+}$ tri-doped $Na_5Y_9F_{32}$ crystals.

In order to further evaluate the laser performance of 2.0 μm, the fluorescence decay curve of Ho^{3+} : $^5I_7$ level is measured. As illustrated in Fig. 10, the decay curves of NYF-HT and NYF-HTE1 crystals both show double exponential decay behavior. Therefore, the florescence lifetimes of Ho^{3+} : $^5I_7$ level can be fitted with the following expression:

$$I = A_1 \exp\left(\frac{-t}{\tau_1}\right) + A2 \exp\left(\frac{-t}{\tau_2}\right). \tag{7}$$

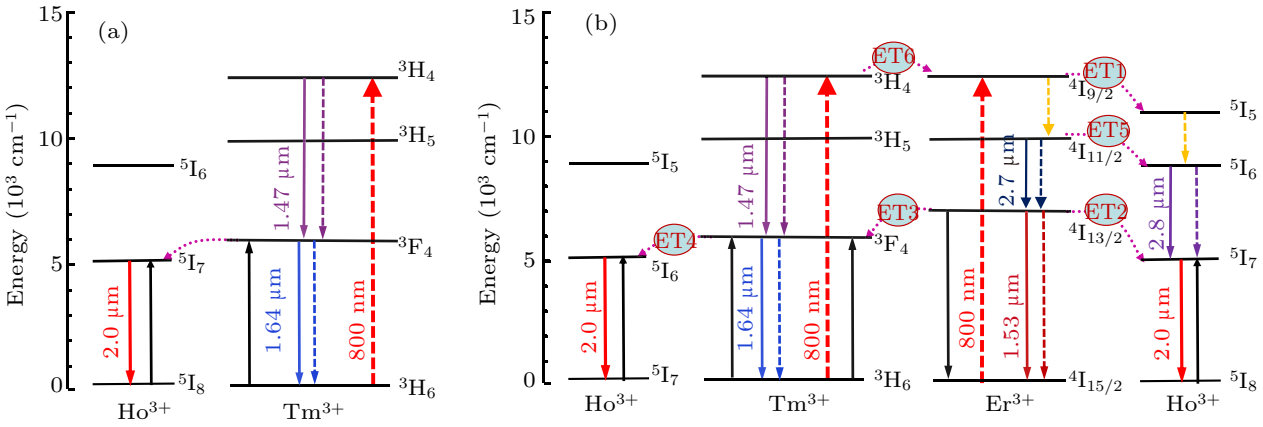

Fig. 9. The energy level diagram and possible energy transfer mechanism in Ho^{3+}/Tm^{3+} co-doped and $Er^{3+}/Ho^{3+}/Tm^{3+}$ tri-doped $Na_5Y_9F_{32}$ crystals.

Then, we calculate the fluorescence lifetime by the following formula:

$$\tau = \frac{A_1\tau_1^2 + A_2\tau_2^2}{A_1\tau_1 + A_2\tau_2}. \tag{8}$$

Figure 10 shows the decay curves of Ho^{3+} : $^5I_7 \rightarrow {}^5I_8$ transition monitored at 2.0-μm region of NYF-HT and NYF-HTE1 crystals excited by 800 nm, the fitted lifetimes is 18.46 ms and 16.28 ms, repetitively. It can be observed that when Er^{3+} ions are added to the Tm^{3+}/Ho^{3+} system, the lifetime of 2.0 μm is reduced from 18.46 ms to 16.28 ms. It can be seen from Fig. 9, the ET1, ET2, ET3, ET5, and ET6 processes are probable to occur between Er^{3+} and Tm^{3+}, Er^{3+} and Ho^{3+} due to the near energy levels. It should be noted that the ET6 process is much easier to take place due to no requiring phonon assistance between Tm^{3+} : $^3H_4$ and Er^{3+} : $^4I_{9/2}$. Under excitation of 800-nm light, the Tm^{3+} ion absorbs the photo of 800 nm by transition from $^3H_6$ to $^3H_4$, and some of energy transfer to Er^{3+} ion by ET6 process. As is known, the ET4 is easier to occur than ET2 process because of the nearer energy difference. The triply doping of Er^{3+} results into the attenuation of the ET4 process and reduction of the lifetime of 2.0 μm. The fluorescence lifetime of NYF-HTE1 crystal at 2.0 μm is much higher than that of germanium tellurate glass reported previously (6.83 ms).[13] The longer radiation lifetime usually reduces the laser oscillation threshold,[26] which indicates that $Er^{3+}/Ho^{3+}/Tm^{3+}$ tri-doped $Na_5Y_9F_{32}$ single crystal is a promising 2.0-μm laser candidate material.

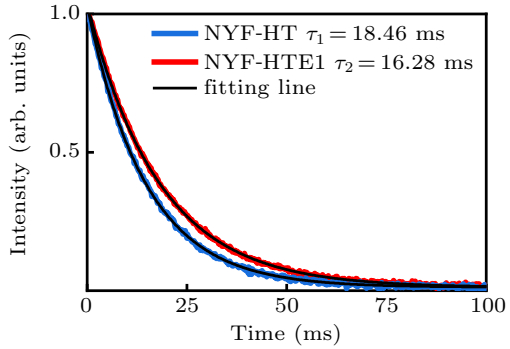

Fig. 10. Decay curves of Ho^{3+} : $^5I_7$ levels monitored at 2.0-μm region of NYF-HT and NYF-HTE1 samples.

Based on the obtained fluorescence lifetimes, we can calculate the energy transfer efficiency between Er^{3+} and Ho^{3+} in $Er^{3+}/Ho^{3+}/Tm^{3+}$ tri-doped $Na_5Y_9F_{32}$ single crystal by the following equation[29]

$$\eta_t = 1 - \frac{\tau_{DA}}{\tau_A}, \tag{9}$$

where τ_A and τ_{DA} are the lifetime of the Ho^{3+} : $^5I_7$ level in NYF-HT crystal and the Ho^{3+} : $^5I_7$ level in NYF-HTE1 crystal, respectively. The efficiency of ET2 process from Er^{3+} : $^4I_{13/2}$ to Ho^{3+} : $^5I_7$ is calculated to be 11.81%. It suggests that the process of Er^{3+} to Ho^{3+} makes a part of the contribution of transfer energy to Ho^{3+} ion together with the energy transfer process of Tm^{3+} to Ho^{3+}, resulting into further enhancement of 2.0 μm.

4. Conclusion

Our experiments demonstrated that the 2.0-μm emission intensity of Tm^{3+}/Ho^{3+} co-doped $Na_5Y_9F_{32}$ single crystal can be further enhanced by introduction of Er^{3+} into the system under 800-nm excitation. The optimized doping concentration of Er^{3+} is ∼ 1 mol% for Tm^{3+} (∼ 1 mol%), Ho^{3+} (∼ 0.8 mol%)-doped $Na_5Y_9F_{32}$ crystal to reach a maximum fluorescence emission of 2.0 μm. The calculated maximum absorption and emission cross-sections at 2.0 μm for $1Er^{3+}/0.8Ho^{3+}/1Tm^{3+}$ tri-doped $Na_5Y_9F_{32}$ crystal are 2.86×10^{-21} cm^2 and 5.26×10^{-21} cm^2, respectively. Meanwhile, the fluorescence lifetimes of $1Er^{3+}/0.8Ho^{3+}/1Tm^{3+}$ tri-doped $Na_5Y_9F_{32}$ crystal is 18.46 ms. The efficiency of ET2 progress is calculated to be 11.81% according to the measured fluorescence lifetimes. Consequently, the excellent luminous properties suggest that $Er^{3+}/Ho^{3+}/Tm^{3+}$ tri-doped $Na_5Y_9F_{32}$ crystals are attractive and significant materials for 2.0-μm lasers.

Acknowledgment

Benli Ding prepared the samples and wrote the article. Xiong Zhou and Jianli Zhang carried out relevant experimental measurements. Xia Haiping embellished and checked the article. Hongwei Song and Baojiu Chen assisted the data analysis. All authors contributed to the general discussion.

References

[1] Yang S, Xia H P, Jiang Y Z, Jiang D S, Wang C, Feng Z G, Zhang J, Gu X M, Zhang J L, Jiang H C and Chen B J 2015 *Chin. Phys. B* **24** 067802
[2] Yao B Q, Zheng L L, Yang X T, Wang T H, Duan X M, Zhao G J and Dong Q 2009 *Chin. Phys. B* **18** 1009
[3] Gao S F, Xu S and Tu C Y 2018 *Opt. laser Technol.* **111** 775
[4] Zhang Y Z, Xu B, Zhang Y S, Liu Y Y, Xu H Y, Cai Z P and Tu C Y 2019 *J. Lumin.* **211** 96
[5] Xiong R, Shi J, Tang W F and Tian D C 2001 *Chin. Phys. B* **10** 52
[6] Simondi-Teisseire B, Viana B, Lejus A M and Vivien D 1997 *J. Lumin.* **72–74** 971
[7] Hu J X, Zhao Y, Chen B J, Xia H P, Zhang Y P and Ye H Q 2019 *J. Lumin.* **205** 500
[8] Qiao Y, Zhou X, Zhang J L, Xia H P, Song H W and Chen B J 2020 *J. Rare Earths*
[9] Li X Y, Peng Y Z, Wei X T, Yuan S, Zhu Y W and Chen D Q 2019 *J. Lumin.* **210** 182
[10] Zhang J P, Zhang W J, Jian Y, Qi Q and Zhang Q Y 2013 *J. Am. Ceram. Soc.* **96** 3836
[11] Jackson S D, Bugge F and Erbert G 2007 *Opt. Lett.* **32** 2496
[12] Jackson S D 2009 *Laser & Photon. Rev.* **3** 466
[13] Lu Y, Cai M Z, Cao R J, Tian Y, Huang F F, Xu S Q and Zhang J J 2016 *Mater. Res. Bull.* **84** 124

[14] Maroni P, Palatella L, Toncelli A and Tonelli M 2001 *J. Cryst. Growth* **229** 497
[15] Zhang P X, Chen Z Q, Hang Y, Li Z, Yin H, Zhu S Q and Fu S H 2017 *Infrared Phys. Technol.* **82** 178
[16] Yang L L, Tang J F, Huang J H, Gong X H, Chen Y J, Lin Y F, Luo Z D and Huang Y D 2013 *Opt. Mater.* **35** 2188
[17] Ding B L, Zhou X, Zhang J L, Xia H P, Song H W and Chen B J 2020 *J. Lumin.* **223** 117254
[18] Li C, Zhang Y, Zhang X J, Zeng F M, Mauro T and Liu J H 2011 *J. Rare Earth.* **29** 592
[19] Tian Y, Xu R R, Hu L L and Zhang J J 2011 *Opt. Lett.* **36** 3218
[20] Peng B O and Izumitani T 1995 *Opt. Mater.* **4** 797
[21] Mccumber D E 1964 *Phys. Rev.* **136** A954
[22] Chen R, Tian Y, Li B P, Wang F C, Jing X F, Zhang J J and Xu S Q 2015 *Opt. Mater.* **49** 116
[23] Florez A, Oliveira S L, Flórez M, Gómez L A and Nunes L A O 2006 *J. Alloys Compd.* **418** 238
[24] Cai M Z, Zhou B, Wang F C, Tian, Zhou J J, Xu S Q and Zhang J J 2015 *Opt. Mater. Express* **5** 1431
[25] Zou X L and Toratani H S 1996 *J. Non-Crystal Solids* **195** 113
[26] Wang M, Yi L X, Wang G N, Hu L L and Zhang J J 2009 *Solid State Commun.* **149** 1216
[27] Qiao Y, Zhou X, Zhang J L, Xia H P, Song H W and Chen B J 2020 *J. Alloys Compd.* **824** 153987
[28] Feng X, Tanabe S and Hanada T 2001 *J. Appl. Phys.* **89** 3560
[29] Zhu Z J, Li J F, You Z Y, Wang Y, Lv S Z, Ma En, Xu J L, Wang H Y and Tu C Y 2012 *Opt. Lett.* **37** 4838